ACS Catalysis

pubs.acs.org/acscatalysis Research Article

Isolated Cr Active Centers in the Beta Zeolite Framework for Propane Dehydrogenation

Zhiqiang Qiu, Zhong-Pan Hu,* Junyu Liu, Jingfeng Han, Shiyu Xia, Min Li, Yang Zhao, Jingrun Chen, Svetlana Mintova, Yingxu Wei,* and Zhongmin Liu

Cite This: *ACS Catal.* 2025, 15, 16539−16549 Read Online

ABSTRACT: Conventional supported metal catalysts in propane dehydrogenation (PDH) face critical challenges due to sintering-induced deactivation at high reaction temperatures. Herein, we develop a series of highly stable atomically dispersed metal-Beta catalysts by embedding single metal atoms (such as V, Cr, Fe, Zn, and Ga) into the dealuminated H-Beta zeolite framework. Unlike the pristine H-Beta zeolite with Brønsted acid sites, the embedded metals possess a distorted tetrahedral structure and typical Lewis acidic properties, which exhibit good C−H bond activation rather than C−C bond activation observed on Brønsted acid sites. Among these metal-Beta zeolites, the Cr-Beta zeolite with an ultralow density of ∼128 framework atoms per Cr atom exhibits notable performance in PDH. Through HAADF-STEM, X-ray absorption spectroscopy (XAS), and isotope labeling FTIR, the local coordination environment of framework-embedded Cr species is unambiguously identified as a distorted tetrahedral geometry $\{(\equiv SiO)_3Cr\cdots(HO-Si\equiv)\}$ with three Cr−O−Si bonds and one Cr···OH−Si linkage. Kinetic investigations and deuterium-labeling results demonstrate that propane activation occurs on isolated Cr Lewis sites with adjacent O atoms that facilitate the reception and release of hydrogen species. These findings provide valuable strategies for the rational design of supported metal catalysts for alkane activation and offer great insights into recognizing the local coordination structures of heteroatoms in zeolites.

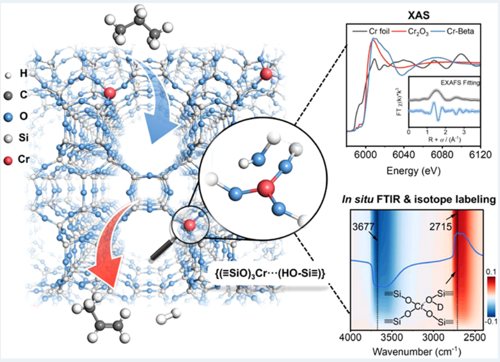

KEYWORDS: *propane dehydrogenation, metal-zeolite, mechanism, Cr species, deuterium-labeling technique*

■ INTRODUCTION

Zeolites are an important class of crystalline materials with unique channel/cavity structures, tunable acidity, and good thermal stability, which have been widely applied in a wide variety of commercial processes, such as adsorptive separation/purification, fluid catalytic cracking (FCC), and methanol-to-olefins (MTO).[1−3] With well-defined framework structures and high surface area, zeolites have proven to be fantastic scaffolds for metal species confined in their matrix spatially and electrostatically, leading to multiple types of catalytic sites with specific locations in these metal-zeolite materials,[4,5] which have achieved great success in heterogeneous catalytic applications, such as dehydrogenation,[6,7] hydrogenation,[8,9] and oxidation.[10] It is known that the local electric field within zeolite channels or cages not only changes the electronic structures of metal active sites but also acts on the guest molecules in specific reactions, in which the active centers and the surrounding microenvironment can work together in the process of adsorption and catalysis, generating unique properties.[2,6,11−13]

Recently, metal-zeolites with isolated metal active sites located in framework T sites[7,14,15] (Co-MFI[6,16] and Zn-MFI[17]) or at extraframework positions[18,19] (Fe-BEA[20−22] and Cu-CHA[23−25]) exhibit great performance for alkane activation. These metal-zeolite materials exhibit remarkable catalytic performance toward alkane activation and maximize the atomic utilization efficiency of metals. They also bridge the gap between heterogeneous and homogeneous catalysis, revealing many parallels to enzyme catalysis with coordinated unsaturated active centers, which differ from subnanoscale and microscale conventional catalysis.[6,9,11,12] Unraveling the isolated metal active sites at the atomic-scale level will illuminate pathways for examining the structure-activity/selectivity relationships, as well as the mechanisms governing these sites in various C−H bond activation processes.[26,27]

Chromium-based catalysts demonstrate high propane conversion and propene selectivity, which are important commercial catalysts for propane dehydrogenation (PDH) and have been extensively studied for decades.[28−30] The structure of the active centers of Cr-based catalysts has sparked

Received: June 17, 2025
Revised: September 8, 2025
Accepted: September 9, 2025
Published: September 16, 2025

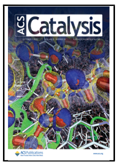

https://doi.org/10.1021/acscatal.5c04181
ACS Catal. 2025, 15, 16539−16549

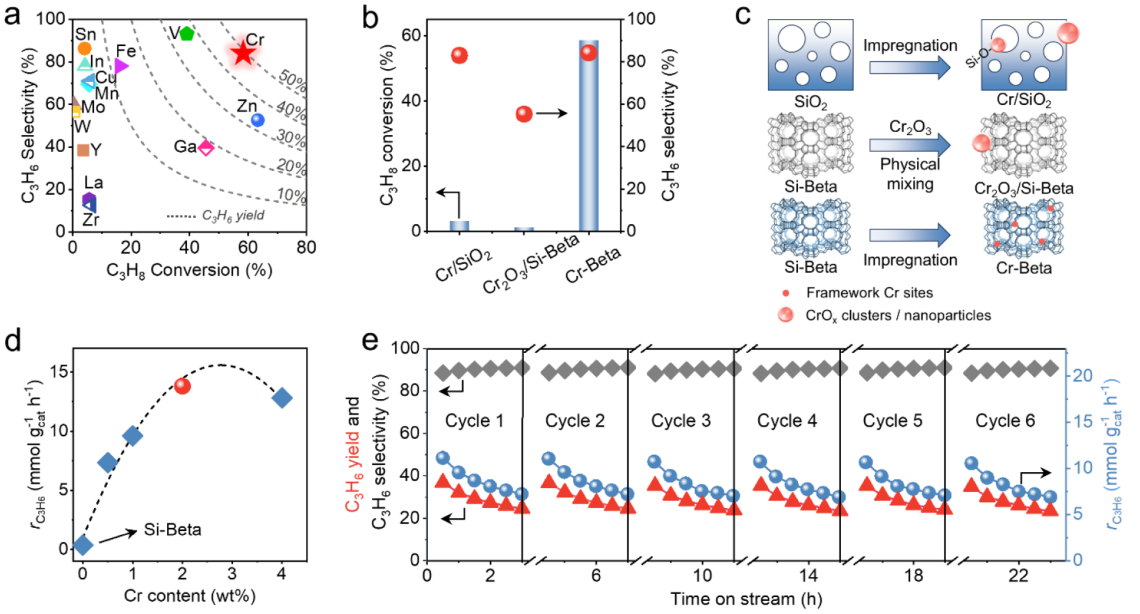

Figure 1. PDH reaction performance over M-Beta catalysts. (a) C_3H_8 conversion and C_3H_6 selectivity of M-Beta at 600 °C, and dotted line is the corresponding propylene yield contour curve created by the Origin software. (b) PDH reaction activity over different Cr-based catalysts. (c) Diagram illustrating the dispersion of Cr species through various introduction methods. (d) Initial C_3H_6 formation rates over Cr-Beta with different Cr loadings. Reaction conditions for (a, b, d): 0.3 g of catalyst, 600 °C, WHSV = 1.18 h^{-1}, 10% C_3H_8 in Ar. (e) PDH performance over the Cr-Beta catalyst during six reaction-regeneration cycles. Regeneration conditions: 600 °C, air (30 mL/min), 20 min.

heated debate owing to the variable valence state, aggregation degree, and the position of Cr species on the support.[10,31−33] It is widely accepted that highly dispersed Cr species are beneficial in the PDH process as the catalytic activity drops when Cr_2O_3 nanoparticles start forming.[28,30] Early discussions on the chromium species' active center focused on CrO_x/SiO_2 catalysts for the important commercial use in propane dehydrogenation.[28] This kind of catalyst, prepared by the traditional impregnation method, mainly forms isolated hexavalent chromates or mono-oxo CrO_5 species.[34] When chromium-based catalysts are used for dehydrogenation reactions, Cr^{VI} species are easily converted to the reduced state of Cr^{II} or Cr^{III}.[10] Copéret et al. developed Cr^{III}/SiO_2 catalysts via metal-organic surface grafting, demonstrating that isolated Cr^{III} sites are covalently bonded to two or three O−Si groups from the silica surface.[35] However, the surface of silica is relatively complex, and its heterogeneity may increase the difficulty in characterizing the active center structure. In recent years, isolated Cr species incorporated into the zeolite framework have exhibited high activity in propane activation, as seen in systems such as Cr-MCM-41,[33] Cr-Beta,[36,37] and Cr-MFI[10,15]. A well-defined catalyst that utilizes the unique framework of zeolites to anchor metal sites combines the advantages of the precise structural control and the high catalytic efficiency to heterogeneous catalysis.[26,38,39] Numerous studies on the structural analysis of Cr isolated sites in single-atom catalysts (SACs)[40] have been reported, with Cr species anchored on metal-organic framework (MOF)[41] and graphitic carbon nitride,[42] while only a limited number of studies have focused on elucidating the detailed structure of isolated Cr active sites within metal-zeolite systems.

In early reports, Wachs et al.[43] combined Raman spectroscopy and DFT calculations and proposed that isolated Cr^{VI} dioxo and Cr^{III} mono-oxo structures on framework Al anchoring sites were the dominant species under most conditions. Dzwigaj et al.[44,45] and Wang et al.[36] further provided spectroscopic insights into M−O and M═O vibrations of Cr species incorporated into the Beta zeolite framework. Nevertheless, direct evidence for the precise structure of isolated Cr sites in metal-zeolite systems, as well as molecular-level insights into the PDH mechanism, remains scarce.

Over the past few decades, the synchrotron-based X-ray absorption spectroscopy (XAS) technique has been considered one of the most powerful and advanced characterization techniques by providing atomic-level information on the structure, coordination environments, and electronic properties of zeolite-confined metal species.[27,46−48] Besides, *operando* IR spectroscopy is another ubiquitous, informative, and versatile characterization method in the field of heterogeneous catalysis, which can be used to probe functional groups of metal-containing zeolites and determine the nature, location, and accessibility of active sites through probe molecules and isotope labeling technology.[26,49,50] In addition, the combination of other multiple technologies, e.g., high-angle annular dark-field scanning transmission electron microscopy (HAADF-STEM), X-ray diffraction (XRD), and UV−visible spectroscopy, allows us to achieve an in-depth understanding of metal-zeolite catalysts more comprehensively.

Based on the above considerations, a series of M-Beta zeolites with framework-isolated metal atoms were synthesized via a postsynthesis method, with Cr-Beta catalysts demonstrating the best PDH performance. The structure of Cr sites was identified by combining XAS, HAADF-STEM, XRD, UV−vis, CD_3CN-FTIR, and H-D exchanged FT-IR techniques, revealing that the isolated Cr active center possesses a pseudotetrahedral structure of $\{(\equiv SiO)_3Cr\cdots(HO-Si\equiv)\}$. The unique coordination structure of the Cr active center and the local microenvironment formed within the zeolite account for the exceptional PDH performance of Cr-Beta.

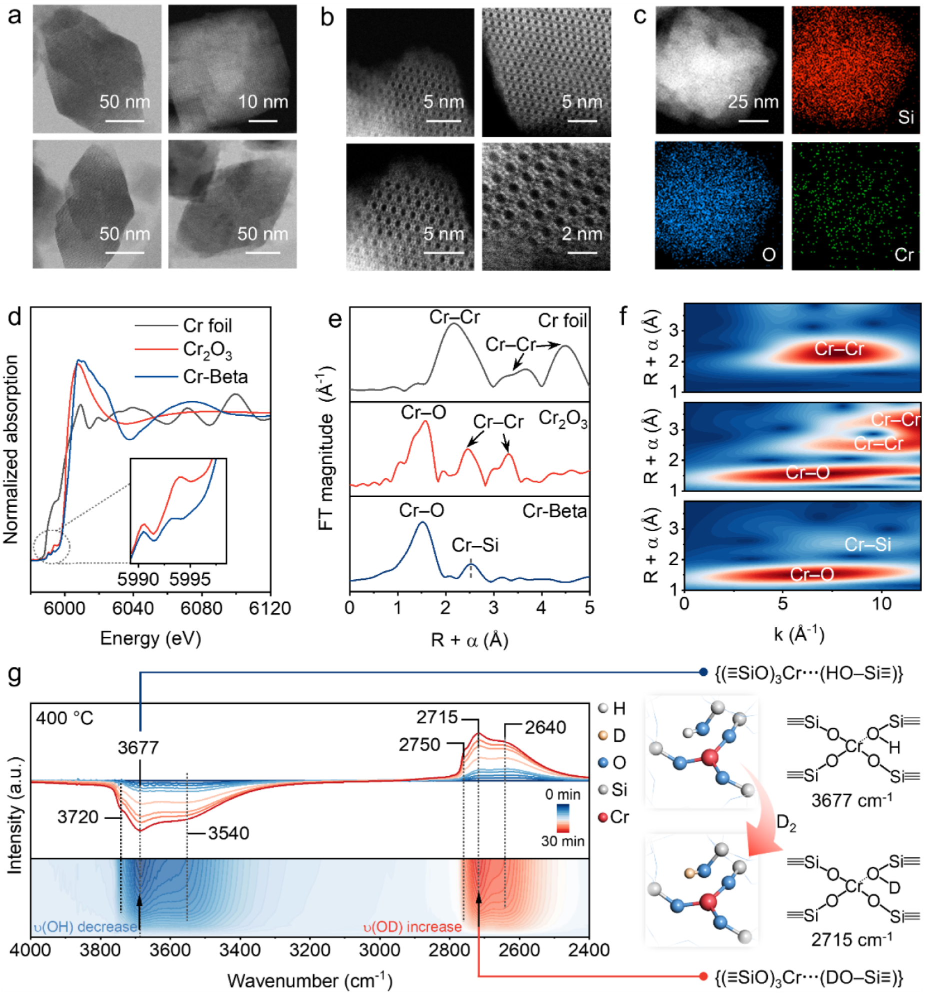

Figure 2. Identification of the local coordination structure of the framework Cr site over Cr-Beta. (a, b) HAADF-STEM and (c) EDS elemental mapping images of the Cr-Beta zeolite. (d) Cr K-edge XANES spectra (Cr-Beta was pretreated with 10% H_2/Ar at 600 °C), (e) corresponding FT k^2-weighted EXAFS spectra, and (f) wavelet-transformed (WT) EXAFS oscillation spectra of Cr foil, Cr_2O_3, and Cr-Beta. (g) H_2/D_2 switching experiment of FT-IR over Cr-Beta at 400 °C (10% D_2/Ar 20 mL/min) and the local structure of the framework Cr sites over Cr-Beta.

RESULTS AND DISCUSSION

Construction of M-Beta Zeolites. In this work, we synthesize a series of M-Beta (M = V, Cr, Fe, Zn, Ga) zeolites via metal-atom incorporation into dealuminated Beta zeolite (Si-Beta) and demonstrate the successful embedding of metal atoms into the BEA zeolite framework. Typically, Beta zeolite (H-Beta) was dealuminated by using concentrated HNO_3, followed by centrifugation and drying to remove Al atoms from the zeolite framework. Subsequently, an equivalent metal atom loading (Si/M = 40, ~128 framework atoms per metal atom) was incorporated into the Beta zeolite framework via the incipient wetness impregnation method with dealuminated Beta zeolite (Si-Beta) and various metal nitrates to obtain M-Beta (Details are provided in the Supporting Information, and all samples were calcined before characterization). N_2-sorption results show that the dealumination process has minimal impact on the pore structures of Beta zeolites (Table S1 and Figure S1), while ^{27}Al NMR (Figure S2) and NH_3-TPD (Figure S3) confirm the almost complete removal of Al atoms, resulting in a Si/Al ratio of 3800 (Table S1) and a marked reduction in acidic sites.

The changes in silanol groups during the dealumination and metal atom introduction processes were characterized by DRIFT spectroscopy (Figure S4). A prominent absorption band at 3730 cm^{-1} is attributed to isolated silanol groups associated with minor structural defects, while the band at 3590 cm^{-1} corresponds to bridging hydroxyl groups (Si–O(H)–Al).[37,51] After dealumination, the Brønsted acid sites are eliminated, and a new broad band appears at approximately 3540 cm^{-1}, indicating the formation of silanol nests, which correspond to the vacant T atom sites in Si-Beta.[7,52] The subsequent reduction of the band at 3540 cm^{-1} upon introduction of metal species into the Beta zeolite reveals that the internal silanol nests serve as anchoring sites, interacting with metal ions to facilitate the integration of metal atoms into the Beta zeolite framework. X-ray fluorescence (XRF) analysis (Table S2) confirms that the molar loading of metal atoms (Si/M = 40) is consistent across all M-Beta samples. Additionally, the UV–vis spectroscopy (Figure S5) of most M-Beta samples reveals no detectable metal oxide nanoparticles or clusters, supporting the conclusion that the postsynthesis treatment effectively embeds metal atoms into the zeolite framework, resulting in dispersed and isolated active centers (Figure S6). Furthermore, the slight shift observed in the XRD diffraction peak (Figure S7) at 2θ = 22.48° (d_{302} spacing), caused by the cell contraction/expansion of Beta zeolite framework, suggests successful dealumination and metal incorporation according to previous reports,[36,44] which also confirm that metal atoms are successfully anchored into the zeolite framework.

PDH Performance of M-Beta Zeolites. The obtained M-Beta (M = V, Cr, Fe, Zn, Ga) catalysts were utilized for PDH, with Cr-Beta exhibiting the highest C_3H_6 yield of ~50% (Figure 1a and Table S3) and the lowest PDH reaction activation energy (~92.0 kJ/mol) barrier (Figure S8) among the M-Beta catalysts. Furthermore, Cr-Beta outperforms other Cr/SiO_2-based catalysts (Figure 1b) by achieving significantly higher initial C_3H_8 conversion (~58%) and C_3H_6 selectivity (~84%). Tables S4−S7 show the PDH performance for the previously reported Cr-based, Pt-based, and other metal-based catalysts. Notably, Cr-Beta displays a high TOF of 124.2 h^{-1}, which is significantly higher than that of previously reported Cr-based and other metal-based catalysts, demonstrating the superior PDH performance of Cr-Beta. In contrast, Cr/SiO_2 prepared via wet impregnation and Cr_2O_3/Si-Beta synthesized through mechanical mixing (with identical Cr loading) exhibit lower catalytic performance (Figure 1c) due to the formation of Cr_2O_3 nanoparticles confirmed by XRD (Figure S9) and UV−vis spectra (Figure S10), which suggests the embedded Cr sites in the Beta zeolite framework offer superior efficiency and selectivity in the PDH reaction. Figure 1d depicts the variation in initial C_3H_6 formation rates with Cr content in Cr-Beta, which follows a volcano-type trend. When the Cr content exceeds 2 wt %, CrO_x clusters or nanoparticles are generated (Figures S11 and S12), leading to diminished conversion rates. This further substantiates that highly dispersed framework Cr sites exhibit greater reactivity in alkane activation compared to CrO_x clusters or nanoparticles, aligning with prior studies.[31,32] The cycle stability test (Figure 1e) revealed that Cr-Beta with framework Cr species maintains a C_3H_6 formation rate of 10.7 mmol g_{cat}^{-1} h^{-1} and ~85% C_3H_6 selectivity over six cycles. The deactivation rate constant k_d values for Cr-Beta propane conversion rate (rC_3H_8) obtained by fitting the first-order GPLE model is 0.17 h^{-1} (Figure S13). Compared with the deactivation rate of previously reported Cr-, Pt-based, and other metal-based catalysts (Table S8), the incorporation of Cr atoms into the Beta zeolite framework can effectively slow down deactivation, even though Cr sites still deactivate by carbon deposits (Figure S14) as a result of their high activity with deep dehydrogenation. In summary, the comparative analysis of Cr species introduction methods and Cr loading in Cr-Beta highlights that generating isolated Cr species within the Beta framework is crucial for achieving high PDH efficiency.

Identification of the Local Coordination Structure of the Framework Cr Site. The previous subsection demonstrates that incorporating isolated Cr sites into the zeolite framework significantly enhances propane conversion, which is crucial for improving PDH performance. Consequently, identifying the coordination structure of the framework Cr sites and recognizing the surrounding microenvironment of active sites confined in the zeolite are essential for elucidating the structure-property relationship of heteroatomic zeolites in alkane activation. Herein, we employ a range of characterization techniques to ascertain the precise structure of the framework Cr sites.

The uniform distribution of Cr species in Cr-Beta was first examined through high-angle annular dark-field scanning transmission electron microscopy (HAADF-STEM) and energy-dispersive X-ray spectroscopy (EDS) mapping (Figure 2c). The microporous channel system of the *BEA structure stacked by polymorph A and polymorph B (Figures 2b and S15) is clearly observed, which also demonstrates that Cr-Beta exhibits high crystallinity without CrO_x clusters or nanoparticles. The HAADF-STEM results of spent Cr-Beta (Figure S16) also demonstrate no aggregation of Cr species after the reaction, which indicates that the framework Cr site is relatively stable during PDH reaction. The coordination environment of the framework Cr sites was then investigated by UV−vis spectroscopy (Figure S12). Two prominent bands, centered at 270 and 360 nm, appear as the dominant absorption bands, corresponding to the ligand-to-metal charge transfer transitions $1T_2 \leftarrow 1A_1$ ($1t_1 \rightarrow 7t_2$ and $6t_2 \rightarrow 2e$) and $1T_2 \leftarrow 1A_1$ ($1t_1 \rightarrow 2e$), respectively.[31,36,53] Additionally, a distinct absorption band at 470 nm, characteristic of distorted tetrahedral Cr species, indicates the presence of isolated tetrahedral Cr species embedded within the BEA framework. In contrast, Cr_2O_3 nanoparticles with octahedral symmetry were detected in Cr/SiO_2, Cr_2O_3/Si-Beta, and Cr-Beta with elevated Cr loading (>4 wt %), as evidenced by a broad absorption band centered at 600 nm in the UV−vis spectra.

In addition, the detailed structure and local environment of Cr species in Cr-Beta were identified by Cr K-edge XAS (Figures 2d−f and S17). Cr foil and Cr_2O_3 are compared as references to distinguish Cr−Cr and Cr−O−Cr bonding environments. The X-ray absorption near-edge structure (XANES) spectrum of prereduced Cr-Beta by H_2 exhibits three peaks at energies of 5990.5, 5993.5, and 6008.7 eV (Figure 2d), which are typical of Cr (III) species. Two small peaks observed in the pre-edge region (see inset in Figure 2d) are attributed to the Cr *d*- and *pz* states, respectively.[10,54,55] The corresponding Fourier transform (FT) k^2-weighted extended X-ray absorption fine structure (EXAFS) spectrum (Figure 2e) and the wavelet-transformed (WT) EXAFS oscillations (Figure 2f) of Cr-Beta, compared with Cr foil and Cr_2O_3, display a dominant peak at 1.56 Å, characteristic of the first shell scattering of O atoms, and a small peak at 2.5 Å, which is attributed to the second shell scattering of Si atoms (nonphase-corrected). The absence of a significant signal above 2.5 Å indicates no obvious polynuclear Cr species. Analysis of Cr K-edge EXAFS of Cr-Beta (Figure S17 and Table 1) reveals a first coordination sphere consisting of three O atoms at 1.96 Å and one O atom at 2.49 Å, with a second shell comprising three Si atoms at 2.8 Å and one Si atom at 3.2 Å, which indicates that Cr-Beta with Cr species incorporated possesses a pseudotetrahedral structure with three Cr−O−Si

Table 1. Structural Parameters[a] of the Cr-Beta Extracted Quantitative EXAFS Curve Fitting

Sample	Path	N[b]	R (Å)[c]	σ^2 (Å^2)[d]	R-factor
Cr-Beta	Cr−O1	3.0	1.96	0.0008	0.0117
	Cr−O2	1.2	2.49	0.0005	
	Cr−Si1	2.9	3.16	0.0090	
	Cr−Si2	1.0	4.20	0.0030	

[a] S_0^2 was fixed at 0.95. $\triangle E_0$ was refined as a global fit parameter, returning a value of (−5.7 ± 1.9) eV. Data ranges: $3 \leq k \leq 10$ Å^{-1}, $1.0 \leq R \leq 4$ Å. The number of variable parameters is 10, out of a total of 13.2 independent data points. R-factor for this fit is 1.17%. All the distances of Cr−O and Cr−Si are derived from the calculated model of Cr-BEA. [b] Coordination number. [c] Distance between adsorber and backscatter atoms. [d] Debye−Waller factor.

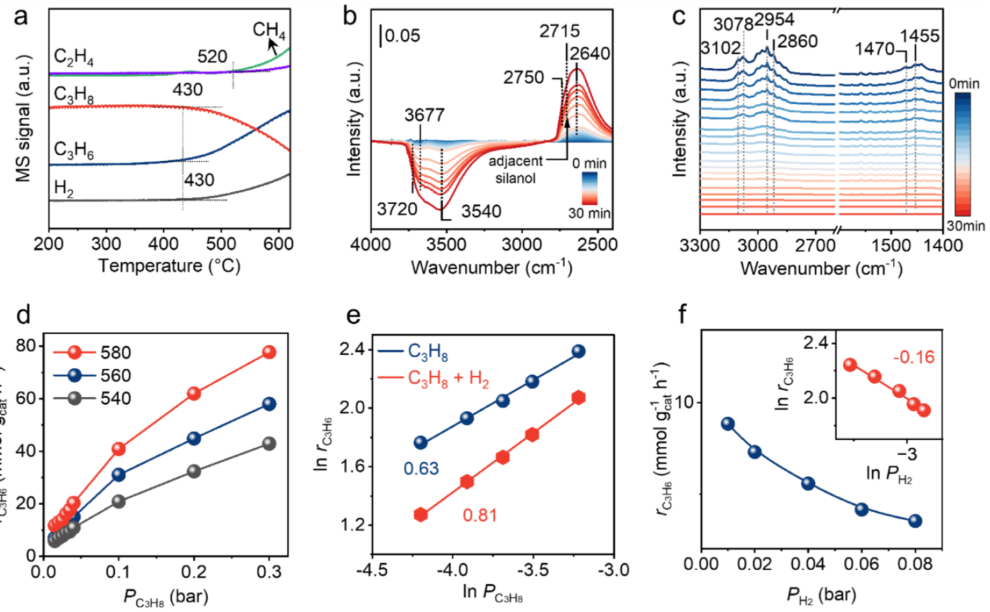

Figure 3. PDH reaction behaviors and kinetics over Cr-Beta. (a) TPSR profiles of the PDH reaction over Cr-Beta. (b) H_2/D_2 switching experiment of FT-IR over Cr-Beta at 300 °C (10% D_2/Ar 20 mL/min). (c) FT-IR spectra of C_3H_6 desorption over Cr-Beta at 100 °C (with Ar at 30 mL/min). (d) Dependence of C_3H_6 formation rates on propane partial pressure over Cr-Beta at different temperatures. (e) Reaction order of propane for the PDH reaction with or without H_2 cofeeding under low propane conversion (<4%). (f) Dependence of C_3H_6 formation rates on H_2 partial pressure over Cr-Beta with H_2 cofeeding.

bonds and one Cr···OH−Si linkage {(≡SiO)$_3$Cr···(HO−Si≡)} (Figure 2g).

To further confirm the structure of the framework Cr sites, H_2/D_2 switching and CD_3CN-absorbed FT-IR experiments are performed. The Cr-Beta was initially treated with H_2 and subsequently exposed to D_2 at 400 °C for 30 min (Figure 2g). After purging D_2, the O−H stretching region (3200−3750 cm^{-1}) decreases in intensity, while the O−D region from 2400 to 2800 cm^{-1} increases. The OD bands at 2750 and 2640 cm^{-1} that appeared upon D atom labeling can be correlated with the consumption of the OH band at 3720 (isolated Si−OH) and 3540 cm^{-1} (Si−OH silanol nest), respectively.[52,56] The band at 2715 cm^{-1} could be ascribed to Si−OD adjacent to Cr Lewis acid sites, which aligns with the identified structure of {(≡SiO)$_3$Cr···(DO−Si≡)}. (Detailed assignments of O−H and O−D bands in Beta zeolite are shown in Table S9 and Figure S18.) Additionally, FTIR experiments of CD_3CN adsorption (Figure S19) on Cr-Beta revealed two bands at 2314 and 2274 cm^{-1}, corresponding to CD_3CN coordinated to Lewis acid Cr sites {(≡SiO)$_3$Cr···(HO−Si≡)} (2314 cm^{-1}) and silanol sites (Si−OH, 2274 cm^{-1}),[6,57] respectively. This indicates that the Cr atoms were successfully incorporated into the BEA framework during the postsynthesis process.

The acidity measurement of Cr-beta by pyridine adsorption/desorption FT-IR spectroscopy (Figure S20) reveals that pyridine adsorbs on Lewis acid sites with dominant bands at 1608, 1490, and 1449 cm^{-1} and interacts with Si−OH at 1446 and 1595 cm^{-1} (which was also found in Si-Beta;[58,59] Figure S20). The absence of discernible vibrations of protonated pyridine near 1550 and 1440 cm^{-1} suggests that the residual Brønsted acid sites after postdealumination are minimal,[60,61] and the silanol adjacent to Cr Lewis sites from Cr···OH−Si linkage exhibits no Brønsted acidity. DFT calculations of pyridine adsorbed on Cr-Beta at the Cr atom or adjacent silanol were simulated (Figure S21 and Table S10). It is shown that pyridine adsorbed on the Cr atom possesses a Δ*G* of −0.36 eV, which is much lower than that adsorbed on the adjacent silanol, suggesting the well-defined Lewis acid site of Cr species. Based on the above characterization results, the local structure of framework Cr sites in Cr-Beta is fully identified as a distorted tetrahedral structure {(≡SiO)$_3$Cr···(HO−Si≡)} with three Cr−O−Si bonds and one Cr···OH−Si linkage (Figure 2g).

PDH Reaction Behaviors and Kinetics Investigation over Cr-Beta. To comprehensively understand the superior PDH performance of the Cr-Beta zeolite, temperature-programmed surface reaction (TPSR) studies were performed on Cr-Beta under a controlled C_3H_8 flow (Figure 3a). The signals corresponding to C_3H_8 consumption and the formation of C_3H_6 and H_2 emerge simultaneously at a relatively low temperature of 430 °C, demonstrating that Cr-Beta exhibits remarkable C−H bond activation capabilities. Additionally, no obvious CH_4 and C_2H_4 were detected before the temperature of 520 °C, indicating high C_3H_6 selectivity in the PDH reaction on Cr-Beta. Within the PDH process, the activation of the C−H bond conventionally marks the initiation of the reaction, succeeded by the cleavage of the second C−H bond and the subsequent desorption of C_3H_6 and H_2, in which the dissociation of the C−H bond and combination of hydrogen species play a pivotal role in driving the reaction pathway.

H_2 dissociation over Cr-Beta was examined by in situ FT-IR spectroscopy at a comparatively low temperature (300 °C, Figure 3b). It was observed that H atoms in silanol groups adjacent to Cr Lewis sites {(≡SiO)$_3$Cr···(HO−Si≡)} were first swapped, with a broad increasing band appearing at 2715 cm^{-1}. In contrast, the O−H vibrational intensity of isolated silanol (3720 cm^{-1}) remained nearly unchanged, showing no evident H−D exchange at 2750 cm^{-1} (isolated Si−OD) even after 30 min, which markedly differs from the results of D_2 treatment at 400 and 500 °C (Figure S22). The higher temperature required for isolated Si−OH to interact with D_2 indicates a slower D_2 dissociation rate compared to silanol

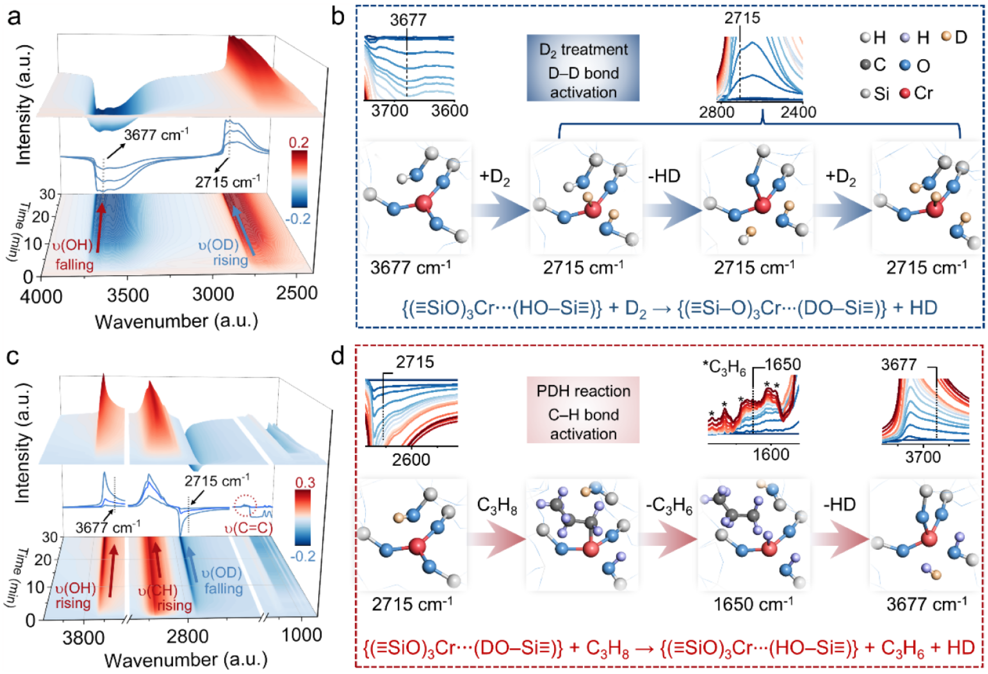

Figure 4. Mechanism investigation of the PDH reaction on the Cr-Beta zeolite. (a) In situ FT-IR of the H_2/D_2 switching experiment at 600 °C over Cr-beta. (b) Partially enlarged diagram of part label a and illustration of D−D bond activation mechanism during D_2 treatement on Cr-Beta. (c) In situ FT-IR of the PDH reaction at 600 °C over D-labeled Cr-beta. (d) Partially enlarged diagram of part label c and illustration of C−H bond activation mechanism during the PDH reaction over D-labeled Cr-Beta. (H_2/D_2 switching experiment: 10% H_2/Ar, then 10% D_2/Ar, 600 °C. PDH reaction: 10% C_3H_8/Ar, 20 mL/min, 600 °C).

groups adjacent to Cr Lewis sites, underscoring the difficulty of D−D bond dissociation over isolated Si−OH due to its weak acidity. Conversely, silanol groups adjacent to the framework Cr sites could be labeled by D atoms even at 300 °C, suggesting that Cr sites directly dissociate D_2, forming new adjacent silanol Si−OD (2715 cm^{-1}) through combination of adjacent Si−OH and Cr−D, releasing HD (Figure S23). This mechanism explains the efficient hydrogen dissociation ability observed at Cr active centers. Furthermore, C_3H_6 desorption was evaluated by FT-IR (Figure 3c), revealing a weak interaction between C_3H_6 and Cr sites, which avoids extensive secondary reactions. In summary, the framework Cr Lewis sites demonstrate remarkable C−H bond activation capabilities, efficient hydrogen dissociation processes, and weak interaction with the product C_3H_6, which collectively underpin the superior PDH activity and selectivity.

As for the kinetics of the PDH reaction over Cr-Beta catalysts, Figure 3d illustrates the dependence of the C_3H_6 formation rate on the partial pressure at various temperatures over Cr-Beta. All kinetic data were collected under mild conditions, where propane conversion ranged from 1% to 4% at high space velocities to minimize the influence of secondary reactions and the partial pressure of products. The propylene formation rate curve increases linearly with rising propane partial pressure but begins to deviate as Cr active centers increasingly become occupied. The reaction order for propane and hydrogen at low propane partial pressure was derived from the slopes of the ln r_{C3H6} versus ln P plots (Figure 3e,f). The propane reaction order was determined to be 0.63 for the PDH process, while it increased to 0.81 with H_2 cofeeding, indicating a higher dependence of C_3H_8 partial pressure on C_3H_6 formation rate when H_2 competes with C_3H_8 for adsorption on Cr Lewis acid sites due to their excellent hydrogen dissociation capacity, as mentioned before. Additionally, the hydrogen reaction order was −0.16, which demonstrates a negative effect on C_3H_6 formation, as the presence of hydrogen not only occupies Cr active sites but also promotes the reverse dehydrogenation reaction, ultimately decreasing the rate of C_3H_6 production.

The kinetic experimental results demonstrate that the isolated Cr sites present a lower initiation temperature for H_2 dissociation (~300 °C) than C−H bond activation in propane (~430 °C), indicating that the former is significantly easier and thus a rapid step. Meanwhile, the desorption of C_3H_6 at Cr sites is also fast, as illustrated by the C_3H_6 desorption FT-IR spectra and the high C_3H_6 selectivity of the PDH reaction. These findings indicate that the activation of the C−H bond is the possible rate-determining step (RDS) in the entire dehydrogenation process. In addition to this assumption, our estimated rate equations (Supplementary note) closely match the actual reaction orders, indicating that the first C−H bond activation is the most likely RDS. According to the derived equations and reaction orders, the reaction order for propane in the PDH process depends on the proportion of unoccupied framework Cr sites, whereas the reaction order for hydrogen is determined by the proportion of Cr sites occupied with hydrogen species.

Mechanism Investigation of the PDH Reaction over Cr-Beta. To investigate the intrinsic mechanism of the PDH reaction over isolated framework Cr sites, in situ FT-IR measurements were conducted in conjunction with isotope labeling techniques to examine the activation of the H−H bond and the C−H bond during the PDH process. Initially, in situ FT-IR experiments were performed over Cr-Beta at 600 °C by sequentially purging H_2 and D_2. Upon introducing H_2 to the Cr-Beta catalysts following Ar pretreatment, the O−H vibration of isolated silanol increased (3733−3720 cm^{-1}), and the band of O−H band at 3677 cm^{-1} emerged within 20 min

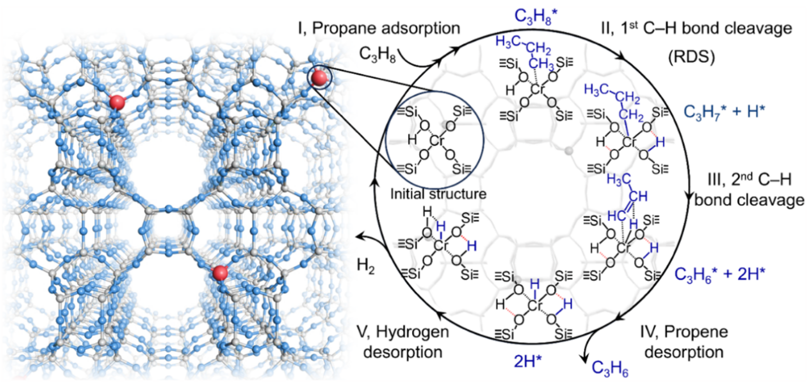

Figure 5. Proposed catalytic cycle of the PDH reaction over the Cr-Beta zeolite.

(Figure S24), possibly indicating H_2 dissociated over framework Cr Lewis sites, leading to an increase in adjacent silanol. The Cr-Beta catalysts were subsequently treated with 10% D_2/Ar after purging H_2, and the in situ IR spectra of O−H and O−D regions in 30 min are shown in Figure 4a. In the partially enlarged diagram (Figure 4b), the peak intensity of the O−H bond at 3677 cm^{-1} which is also observed during H_2 dissociation, declines, while a broad vibration of the O−D bond at 2715 cm^{-1} grows, indicating that H atoms in the adjacent silanol groups are substituted by D atoms.

As we demonstrated earlier, the isolated framework Cr sites exhibit a pseudotetrahedral structure $\{(\equiv SiO)_3Cr\cdots(HO-Si\equiv)\}$ and the peak at 2715 cm^{-1} is attributed to the O−D bond of the adjacent silanol groups to the Cr sites substituted by the D atom $\{(\equiv SiO)_3Cr\cdots(DO-Si\equiv)\}$. Specifically, D_2 dissociates heterolytically on Cr sites, where the Cr atom accepts one D atom and the neighboring oxygen atom (Cr−O−Si) accepts another one, which may weaken the bond between Cr and the nearby oxygen atom (Cr−O bond), forming a new D-labeled adjacent silanol group $\{(\equiv SiO)_3Cr\cdots(DO-Si\equiv)\}$ followed by the rapid elimination of HD. After continued exposure to D_2, an intermediate forms with two adjacent silanol groups over Cr sites $\{(\equiv SiO)_2Cr-D(DO-Si\equiv)_2\}$, resulting in a further increase of the O−D band at 2715 cm^{-1} (Figure 4b).

Additionally, in situ FT-IR spectra of the PDH process were obtained over D-labeled Cr-Beta (Figure 4c). With the introduction of propane, the infrared difference spectra show a significant increase in the C−H bond region, accompanied by an elevation of the adjacent silanol at 3677 cm^{-1}, which is produced by the first dissociation of the C−H bond of propane. This suggests that C_3H_8 decomposes into Cr−C_3H_7 and transfers the first H* to the adjacent oxygen, forming the Cr···HO−Si species (3677 cm^{-1}). The reduced band at 2715 cm^{-1} indicates that the D atoms of D-labeled adjacent silanol (Cr···DO−Si) are consumed during the PDH reaction. Simultaneously, surface propylene (C_3H_6*) species are generated by the second C−H bond cleavage of propane, as C═C vibrational modes[62] at 1650 cm^{-1} characteristic of molecular propene, were observed (Figure 4c,d).

Considering the electronegative properties exhibited by different H atoms[6] during the PDH process (e.g., the H atom bonded to oxygen atoms is positively charged, whereas the H atom attached to the Cr atom (Cr−H) exhibits more electronegative properties), the combination between $H^{\delta+}$ and $H^{\delta-}$ in $\{(\equiv SiO)_2CrH^{\delta-}(H^{\delta+}O-Si\equiv)_2\}$ leads to the release of H_2 molecule. Therefore, the D atom from D-labeled silanol (Si−$OD^{\delta+}$) and Cr−$H^{\delta-}$ species combines, resulting in the decline of the vibration band at 2715 cm^{-1} (Figure 4d), which completes the entire catalytic cycle of the PDH process over the framework Cr sites and restores the initially distorted tetrahedral structure $\{(\equiv SiO)_3Cr\cdots(HO-Si\equiv)\}$.

Based on the mechanistic investigation conducted via in situ FT-IR and kinetic analysis, the catalytic cycle of PDH over Cr-Beta was proposed (Figure 5). The PDH reaction is initiated over the framework Cr Lewis sites, which were identified in Section Identification of the Local Coordination Structure of the Framework Cr Site with the distorted tetrahedral structure $\{(\equiv SiO)_3Cr\cdots(HO-Si\equiv)\}$. First, propane is adsorbed on the Cr atom, followed by a heterolytic C−H bond activation step of the first C−H bond on the Cr−O−Si site, forming a Cr−C_3H_7 intermediate and Cr···HO−Si species, which suggests that the neighboring oxygen accepts hydrogen while weakening the Cr−O bond. Then, C_3H_6 is formed through β−H transfer from the alkyl group to the Cr atom, resulting in Cr−H species with a second C−H bond cleavage. After the quick departure of C_3H_6, the desorption of hydrogen is facilitated by the coupling of two hydrogen atoms of the Si−O−$H^{\delta+}$ and Cr−$H^{\delta-}$ species. Throughout the catalytic cycle, the neighboring oxygen atoms of Cr sites accept hydrogen from C_3H_8, while oxygen atoms from adjacent silanol continuously release hydrogen, acting as hydrogen species transfer stations, thereby sustaining the dehydrogenation cycle. As highlighted in our previous report,[6] similarly in this work, the coordinated oxygen atom of the isolated Cr Lewis acid site confined in the zeolite is possibly polarized by the Cr site owing to the hybridization of 3d (Cr) and 2p (O) orbitals, making it a bridge for electron transfer.

CONCLUSIONS

In this study, we constructed a series of metal-zeolite catalysts via a postsynthesis method, incorporating metal atoms into the Beta zeolite framework, and employed these catalysts for the PDH reaction. Among the M-Beta catalysts, Cr-Beta demonstrated the highest C_3H_6 yield (~50%) at 600 °C with a propane space velocity of 1.18 h^{-1} and the lowest PDH reaction activation energy (~92.0 kJ/mol). The precise coordination structure of framework Cr sites was evaluated by XRD, HAADF-STEM, UV−vis, XAS, Py-IR, CD_3CN-IR spectroscopy, and H_2/D_2 switching experiments, revealing that Cr atoms were uniformly incorporated into the Beta zeolite framework with a pseudotetrahedral structure of $\{(\equiv SiO)_3Cr\cdots(HO-Si\equiv)\}$, which functions as Lewis acid sites. The exceptional dehydrogenation activity and selectivity of the framework Cr sites are attributed to the high C−H bond activation efficiency, rapid hydrogen dissociation capability, and minimal interaction with the product C_3H_6, as demonstrated by TPSR and H−D exchange experiments. Kinetic studies revealed that the activation of C−H bonds is likely the rate-determining step for the PDH reaction on Cr-Beta, with the dependence on propane partial pressure determined by the proportion of unoccupied framework Cr sites. Furthermore, the PDH reaction mechanism at the unique framework Cr sites was demonstrated by in situ FT-IR experiments aided by isotope labeling techniques. The results indicate that C_3H_8 undergoes initial activation at the Cr site, dissociating the first C−H bond to form Cr−C_3H_7 and Cr···HO−Si species, while the second C−H bond dissociates into Cr−H species, releasing C_3H_6. The catalytic cycle is completed through a combination of surface hydrogen species (Cr−H and Cr···HO−Si) to restore the initial state of {$(\equiv SiO)_3$Cr···(HO−Si≡)}. Crucially, the isolated Cr centers in the Beta zeolite framework facilitate sequential hydrogen abstraction from C_3H_8, and the adjacent O atoms function as hydrogen transfer mediators, ensuring efficient C_3H_6 production. These findings enhance our understanding of Cr-based catalysis in PDH reactions and provide valuable guidance for developing high-performance alkane dehydrogenation catalysts and processes. Isolated Cr species in the Beta zeolite framework, as well-defined active sites together with the unique zeolite microenvironment, contribute to highly efficient PDH performance, which outperforms other metals embedded into Beta zeolite. Besides the electronic properties and coordination structure of metal sites, a profound and systematic study considering the differences in Lewis acid strength of framework metal sites, both experimentally and theoretically, would further explain the superior PDH performance of Cr-Beta catalyst and shed light on the structure-activity relationship of heteroatom zeolite systems in alkane activation reactions.

■ MATERIALS AND METHODS

Materials. All chemicals were obtained as received, without further purification. The following materials were used: Beta zeolite (SiO_2/Al_2O_3 = 25, Nankai University Catalyst Co., Ltd.), SiO_2 (99%, Tianjin Shenneng Technology Co., Ltd.), Chromium(III) nitrate ($Cr(NO_3)_3·9H_2O$, 99%, Sinopharm Chemical Reagent Co., Ltd.). Other nitrate raw materials used in the experiment were purchased from Shanghai Aladdin Biochemical Technology Co., Ltd., including H_4NO_3V, $Mn(NO_3)_2·4H_2O$, $Fe(NO_3)_3·9H_2O$, $Cu(NO_3)_2·3H_2O$, $Zn(NO_3)_2·6H_2O$, $Ga(NO_3)_3·xH_2O$, $Y(NO_3)_3·6H_2O$, $Zr(NO_3)_4·5H_2O$, $MoNa_2O_4$, $In(NO_3)_3·xH_2O$, $SnCl_4·5H_2O$, $La(NO_3)_3·6H_2O$, $Na_2WO_4·2H_2O$.

Methods. The preparation of Si-Beta: The dealuminated Beta zeolite (Si-Beta) was obtained by treating the raw Beta zeolite with concentrated nitric acid at 90 °C for 24 h. After being washed with distilled water, the sample was dried at 120 °C overnight, resulting in the final product, Si-Beta. The Si/Al ratio of Si-Beta was determined to be 3800.

The preparation of M-Beta: Metal-containing -Beta catalysts (M-Beta) were prepared by the liquid-phase incorporation (LPI) method. Specifically, the calculated $M(NO_3)_x·yH_2O$ (the metal salt required to synthesize 2 g of M-Beta (Si/M = 40) was dissolved in 20 mL of deionized water. Then, the desired amount of Si-Beta was added to the nitrate solution, and the mixture was stirred at room temperature for 3 h. The mixture was evaporated at 80 °C under stirring and subsequently dried overnight at 120 °C. Finally, all materials were calcined at 550 °C for 6 h at a heating rate of 2 °C/min.

The preparations of xCr-Beta, xCr/SiO_2, and Cr_2O_3/Si-Beta: Cr-Beta and Cr/SiO_2 with different Cr loadings were prepared by a wet-impregnation method, which was similar to the preparation of M-Beta by choosing Si-Beta and SiO_2 as supports. The Cr_2O_3/Si-Beta sample was prepared by physically mixing Cr_2O_3 and Si-Beta.

Characterization and Catalytic Evaluation. The physicochemical properties of the catalyst and the structures of the active centers were investigated by combining various characterization techniques. The PDH reaction was carried out in a quartz tubular fixed-bed reactor at 600 °C under atmospheric pressure. C_3H_8 conversion and product selectivity were calculated using carbon balance. The Supporting Information provides details of the characterizations and catalytic assessments.

■ ASSOCIATED CONTENT

Supporting Information

The Supporting Information is available free of charge at https://pubs.acs.org/doi/10.1021/acscatal.5c04181.

The experiments, characterization results (N_2−BET, ^{27}Al MAS NMR, and NH_3-TPD of H-Beta and Si-Beta (Figures S1−S3); XRD and UV−vis results of all the M-Beta catalysts (Figures S5−S7); TGA (Figure S14), HAADF-STEM (Figures S15 and S16), CD_3CN-FTIR (Figure S19), Py-FTIR (Figure S20), and D_2-FTIR (Figure S22) characterization results of Cr-Beta), and other supplementary results and discussion of reaction and spectroscopy (PDF)

■ AUTHOR INFORMATION

Corresponding Authors

Yingxu Wei − *National Engineering Research Center of Lower-Carbon Catalysis Technology, Dalian National Laboratory for Clean Energy, iChEM (Collaborative Innovation Center of Chemistry for Energy Materials), Dalian Institute of Chemical Physics, Chinese Academy of Sciences, Dalian 116023, China*; orcid.org/0000-0002-0412-1980; Email: weiyx@dicp.ac.cn

Zhong-Pan Hu − *National Engineering Research Center of Lower-Carbon Catalysis Technology, Dalian National Laboratory for Clean Energy, iChEM (Collaborative Innovation Center of Chemistry for Energy Materials), Dalian Institute of Chemical Physics, Chinese Academy of Sciences, Dalian 116023, China*; Email: huzp@dicp.ac.cn

Authors

Zhiqiang Qiu − *National Engineering Research Center of Lower-Carbon Catalysis Technology, Dalian National Laboratory for Clean Energy, iChEM (Collaborative Innovation Center of Chemistry for Energy Materials), Dalian Institute of Chemical Physics, Chinese Academy of Sciences, Dalian 116023, China; School of Chemical Engineering, University of Chinese Academy of Sciences, Beijing 100049, China*

Junyu Liu − *National Engineering Research Center of Lower-Carbon Catalysis Technology, Dalian National Laboratory for Clean Energy, iChEM (Collaborative Innovation Center of Chemistry for Energy Materials), Dalian Institute of Chemical Physics, Chinese Academy of Sciences, Dalian*

116023, China; School of Chemical Engineering, University of Chinese Academy of Sciences, Beijing 100049, China

Jingfeng Han − *National Engineering Research Center of Lower-Carbon Catalysis Technology, Dalian National Laboratory for Clean Energy, iChEM (Collaborative Innovation Center of Chemistry for Energy Materials), Dalian Institute of Chemical Physics, Chinese Academy of Sciences, Dalian 116023, China;* orcid.org/0000-0001-7775-4183

Shiyu Xia − *National Engineering Research Center of Lower-Carbon Catalysis Technology, Dalian National Laboratory for Clean Energy, iChEM (Collaborative Innovation Center of Chemistry for Energy Materials), Dalian Institute of Chemical Physics, Chinese Academy of Sciences, Dalian 116023, China; School of Chemical Engineering, University of Chinese Academy of Sciences, Beijing 100049, China*

Min Li − *Elettra−Sincrotrone Trieste, Trieste 34149, Italy*

Yang Zhao − *Dalian National Laboratory for Clean Energy (DNL), Dalian Institute of Chemical Physics, Chinese Academy of Sciences, Dalian 116023, P. R. China*

Jingrun Chen − *Shaanxi Hydrogen Energy Research Institute Co. Ltd, Fengxi New City, Shaanxi 712046, China*

Svetlana Mintova − *Laboratoire Catalyse et Spectrochimie (LCS) Normandie Univ, ENSICAEN, UNICAEN, CNRS, Caen 14000, France;* orcid.org/0000-0002-0738-5244

Zhongmin Liu − *National Engineering Research Center of Lower-Carbon Catalysis Technology, Dalian National Laboratory for Clean Energy, iChEM (Collaborative Innovation Center of Chemistry for Energy Materials), Dalian Institute of Chemical Physics, Chinese Academy of Sciences, Dalian 116023, China; School of Chemical Engineering, University of Chinese Academy of Sciences, Beijing 100049, China; State Key Laboratory of Catalysis, Dalian Institute of Chemical Physics, Chinese Academy of Sciences, Dalian 116023, China;* orcid.org/0000-0002-7999-2940

Complete contact information is available at:
https://pubs.acs.org/10.1021/acscatal.5c04181

Notes

The authors declare no competing financial interest.

■ ACKNOWLEDGMENTS

The authors are thankful for the financial support from the National Key R&D Program of China (No. 2022YFE0116000), the National Natural Science Foundation of China (Nos. 22202193, 22472165, 22172166), Innovation Research Foundation of the Dalian Institute of Chemical Physics (DICP), CAS (Nos. DICP I202429, DICP I201926), Open Foundation of State Key Laboratory of Catalysis, DICP, CAS (No. 2024SKL-A-003), the Youth Innovation Promotion Association CAS (2021182). We also thank the staff at the BL14W1 beamline of the Shanghai Synchrotron Radiation Facility for their assistance with the XANES and EXAFS measurements.

■ REFERENCES

(1) Yan, W.; Li, Y.; Xiao, F.; Liu, Z.; Yu, J. The Future of Zeolites. *Chem. Mater.* **2024**, *36* (15), 7103−7105.

(2) Zhang, W.; Lin, S.; Wei, Y.; Tian, P.; Ye, M.; Liu, Z. Cavity-Controlled Methanol Conversion over Zeolite Catalysts. *Natl. Sci. Rev.* **2023**, *10* (9), nwad120.

(3) Chen, G.; Liu, G.; Pan, Y.; Liu, G.; Gu, X.; Jin, W.; Xu, N. Zeolites and Metal−Organic Frameworks for Gas Separation: The Possibility of Translating Adsorbents into Membranes. *Chem. Soc. Rev.* **2023**, *52* (14), 4586−4602.

(4) Xu, Z.; Gao, M.; Wei, Y.; Yue, Y.; Bai, Z.; Yuan, P.; Fornasiero, P.; Basset, J. M.; Mei, B.; Liu, Z.; Zhu, H.; Ye, M.; Bao, X. Pt Migration−Lockup in Zeolite for Stable Propane Dehydrogenation Catalyst. *Nature* **2025**, *643* (8072), 691−698.

(5) Hong, H.; Xu, Z.; Mei, B.; Hu, W.; Fornasiero, P.; Wang, C.; Wang, T.; Yue, Y.; Li, T.; Yang, C.; Cui, Q.; Zhu, H.; Bao, X. A Self-Regenerating Pt/Ge-MFI Zeolite for Propane Dehydrogenation with High Endurance. *Science* **2025**, *388* (6746), 497−502.

(6) Hu, Z.; Qin, G.; Han, J.; Zhang, W.; Wang, N.; Zheng, Y.; Jiang, Q.; Ji, T.; Yuan, Z.; Xiao, J.; Wei, Y.; Liu, Z. Atomic Insight into the Local Structure and Microenvironment of Isolated Co-Motifs in MFI Zeolite Frameworks for Propane Dehydrogenation. *J. Am. Chem. Soc.* **2022**, *144* (27), 12127−12137.

(7) Ni, L.; Khare, R.; Bermejo-Deval, R.; Zhao, R.; Tao, L.; Liu, Y.; Lercher, J. A. Highly Active and Selective Sites for Propane Dehydrogenation in Zeolite Ga-BEA. *J. Am. Chem. Soc.* **2022**, *144* (27), 12347−12356.

(8) Liu, H.; Li, J.; Liang, X.; Ren, H.; Yin, H.; Wang, L.; Yang, D.; Wang, D.; Li, Y. Encapsulation of Pd Single-Atom Sites in Zeolite for Highly Efficient Semihydrogenation of Alkynes. *J. Am. Chem. Soc.* **2024**, *146* (34), 24033−24041.

(9) Chai, Y.; Wu, G.; Liu, X.; Ren, Y.; Dai, W.; Wang, C.; Xie, Z.; Guan, N.; Li, L. Acetylene-Selective Hydrogenation Catalyzed by Cationic Nickel Confined in Zeolite. *J. Am. Chem. Soc.* **2019**, *141* (25), 9920−9927.

(10) Zhou, W.; Felvey, N.; Guo, J.; Hoffman, A. S.; Bare, S. R.; Kulkarni, A. R.; Runnebaum, R. C.; Kronawitter, C. X. Reduction of Cofed Carbon Dioxide Modifies the Local Coordination Environment of Zeolite-Supported, Atomically Dispersed Chromium to Promote Ethane Dehydrogenation. *J. Am. Chem. Soc.* **2024**, *146* (14), 10060−10072.

(11) Chai, Y.; Dai, W.; Wu, G.; Guan, N.; Li, L. Confinement in a Zeolite and Zeolite Catalysis. *Acc. Chem. Res.* **2021**, *54* (13), 2894−2904.

(12) Deng, X.; Yang, D.; Li, W.; Chai, Y.; Wu, G.; Li, L. Chemistry of Coordinatively Unsaturated Centers in Zeolites. *Trends Chem.* **2023**, *5* (12), 892−905.

(13) Chai, Y.; Han, X.; Li, W.; Liu, S.; Yao, S.; Wang, C.; Shi, W.; da-Silva, I.; Manuel, P.; Cheng, Y.; Daemen, L. D.; Ramirez-Cuesta, A. J.; Tang, C. C.; Jiang, L.; Yang, S.; Guan, N.; Li, L. Control of Zeolite Pore Interior for Chemoselective Alkyne/Olefin Separations. *Science* **2020**, *368* (6494), 1002−1006.

(14) Suib, S. L.; Přech, J.; Szaniawska, E.; Čejka, J.-R.-A.-I.-T. (Ti, Sn, Zr, Hf) and Pentavalent (Nb, V, Ta) Metal-Substituted Molecular Sieve Catalysis. *Chem. Rev.* **2023**, *123* (3), 877−917.

(15) De, S.; Ould-Chikh, S.; Aguilar, A.; Hazemann, J. L.; Zitolo, A.; Ramirez, A.; Telalovic, S.; Gascon, J. Stable Cr-MFI Catalysts for the Nonoxidative Dehydrogenation of Ethane: Catalytic Performance and Nature of the Active Sites. *ACS Catal.* **2021**, *11* (7), 3988−3995.

(16) Zhou, H.; Li, H.; Wang, L.; Chu, S.; Liu, L.; Liu, L.; Qi, J.; Ren, Z.; Cai, A.; Hui, Y.; Qin, Y.; Song, L.; Qin, X.; Shi, J.; Hou, J.; Ding, Y.; Ma, J.; Xu, S.; Tao, X.; Li, L.; Yang, Q.; Hu, B.; Liu, X.; Chen, L.; Xiao, J.; Xiao, F. Cobaltosilicate Zeolite beyond Platinum Catalysts for Propane Dehydrogenation. *Nat. Catal.* **2025**, *8* (4), 357−367.

(17) Su, X.; Hu, Z.; Han, J.; Jia, Y.; Xu, S.; Zhang, J.; Fan, D.; Wei, Y.; Liu, Z. Biomolecule-Inspired Synthesis of Framework Zinc in MFI Zeolite for Propane Dehydrogenation. *Microporous Mesoporous Mater.* **2023**, *348*, 112371.

(18) Shan, J.; Li, M.; Allard, L. F.; Lee, S.; Flytzani-Stephanopoulos, M. Mild Oxidation of Methane to Methanol or Acetic Acid on Supported Isolated Rhodium Catalysts. *Nature* **2017**, *551* (7682), 605−608.

(19) Maeno, Z.; Yasumura, S.; Wu, X.; Huang, M.; Liu, C.; Toyao, T.; Shimizu, K. Isolated Indium Hydrides in CHA Zeolites:

Speciation and Catalysis for Nonoxidative Dehydrogenation of Ethane. *J. Am. Chem. Soc.* **2020**, *142* (10), 4820−4832.

(20) Bols, M. L.; Snyder, B. E. R.; Rhoda, H. M.; Cnudde, P.; Fayad, G.; Schoonheydt, R. A.; Van Speybroeck, V.; Solomon, E. I.; Sels, B. F. Coordination and Activation of Nitrous Oxide by Iron Zeolites. *Nat. Catal.* **2021**, *4* (4), 332−340.

(21) Scott, S. L. Bioinspired Methane Oxidation in a Zeolite. *Science* **2021**, *373* (6552), 277−278.

(22) Snyder, B. E. R.; Bols, M. L.; Rhoda, H. M.; Plessers, D.; Schoonheydt, R. A.; Sels, B. F.; Solomon, E. I. Cage Effects Control the Mechanism of Methane Hydroxylation in Zeolites. *Science* **2021**, *373* (6552), 327−331.

(23) Zhang, H.; Li, J.; Wang, D.; Wang, Y.; Xiong, H. A Review on the Active Sites for Direct Oxidation of Methane to Methanol by Copper-Zeolites: Coordination Structure, Formation and Activity. *Coordin Chem. Rev.* **2024**, *503*, 215637.

(24) Sushkevich, V. L.; Palagin, D.; Ranocchiari, M.; Van Bokhoven, J. A. Selective Anaerobic Oxidation of Methane Enables Direct Synthesis of Methanol. *Science* **2017**, *356* (6337), 523−527.

(25) Pappas, D. K.; Borfecchia, E.; Dyballa, M.; Pankin, I. A.; Lomachenko, K. A.; Martini, A.; Signorile, M.; Teketel, S.; Arstad, B.; Berlier, G.; Lamberti, C.; Bordiga, S.; Olsbye, U.; Lillerud, K. P.; Svelle, S.; Beato, P. Methane to Methanol: Structure−Activity Relationships for Cu-CHA. *J. Am. Chem. Soc.* **2017**, *139* (42), 14961−14975.

(26) Zhang, Q.; Gao, S.; Yu, J. Metal Sites in Zeolites: Synthesis, Characterization, and Catalysis. *Chem. Rev.* **2023**, *123* (9), 6039−6106.

(27) Liu, Y.; Su, X.; Ding, J.; Zhou, J.; Liu, Z.; Wei, X.; Yang, H. B.; Liu, B. Progress and Challenges in Structural, in Situ and Operando Characterization of Single-Atom Catalysts by X-Ray Based Synchrotron Radiation Techniques. *Chem. Soc. Rev.* **2024**, *53* (24), 11850−11887.

(28) Sattler, J. J. H. B.; Ruiz-Martinez, J.; Santillan-Jimenez, E.; Weckhuysen, B. M. Catalytic Dehydrogenation of Light Alkanes on Metals and Metal Oxides. *Chem. Rev.* **2014**, *114* (20), 10613−10653.

(29) Chen, S.; Chang, X.; Sun, G.; Zhang, T.; Xu, Y.; Wang, Y.; Pei, C.; Gong, J. Propane Dehydrogenation: Catalyst Development, New Chemistry, and Emerging Technologies. *Chem. Soc. Rev.* **2021**, *50* (5), 3315−3354.

(30) Sun, M.; Hu, Z.; Wang, H.; Suo, Y.; Yuan, Z. Design Strategies of Stable Catalysts for Propane Dehydrogenation to Propylene. *ACS Catal.* **2023**, *13* (7), 4719−4741.

(31) Baek, J.; Yun, H. J.; Yun, D.; Choi, Y.; Yi, J. Preparation of Highly Dispersed Chromium Oxide Catalysts Supported on Mesoporous Silica for the Oxidative Dehydrogenation of Propane Using CO_2: Insight into the Nature of Catalytically Active Chromium Sites. *ACS Catal.* **2012**, *2* (9), 1893−1903.

(32) Santhosh Kumar, M.; Hammer, N.; Rønning, M.; Holmen, A.; Chen, D.; Walmsley, J. C.; Øye, G. The Nature of Active Chromium Species in Cr-Catalysts for Dehydrogenation of Propane: New Insights by a Comprehensive Spectroscopic Study. *J. Catal.* **2009**, *261* (1), 116−128.

(33) Takehira, K.; Ohishi, Y.; Shishido, T.; Kawabata, T.; Takaki, K.; Zhang, Q.; Wang, Y. Behavior of Active Sites on Cr-MCM-41 Catalysts during the Dehydrogenation of Propane with CO_2. *J. Catal.* **2004**, *224* (2), 404−416.

(34) Barzan, C.; Piovano, A.; Braglia, L.; Martino, G. A.; Lamberti, C.; Bordiga, S.; Groppo, E. Ligands Make the Difference! Molecular Insights into Cr^{VI}/SiO_2 Phillips Catalyst during Ethylene Polymerization. *J. Am. Chem. Soc.* **2017**, *139* (47), 17064−17073.

(35) Delley, M. F.; Núñez-Zarur, F.; Conley, M. P.; Comas-Vives, A.; Siddiqi, G.; Norsic, S.; Monteil, V.; Safonova, O. V.; Copéret, C. Proton Transfers Are Key Elementary Steps in Ethylene Polymerization on Isolated Chromium(III) Silicates. *Proc. Natl. Acad. Sci. U. S. A.* **2014**, *111* (32), 11624−11629.

(36) Wang, J.; Zhu, M.; Song, Y.; Liu, Z.; Wang, L.; Liu, Z. Molecular-Level Investigation on Supported CrO_x Catalyst for Oxidative Dehydrogenation of Propane with Carbon Dioxide. *J. Catal.* **2022**, *409*, 87−97.

(37) Michorczyk, P.; Zeńczak-Tomera, K.; Michorczyk, B.; Węgrzyniak, A.; Basta, M.; Millot, Y.; Valentin, L.; Dzwigaj, S. Effect of Dealumination on the Catalytic Performance of Cr-Containing Beta Zeolite in Carbon Dioxide Assisted Propane Dehydrogenation. *J. CO2 Util.* **2020**, *36*, 54−63.

(38) Copéret, C.; Allouche, F.; Chan, K. W.; Conley, M. P.; Delley, M. F.; Fedorov, A.; Moroz, I. B.; Mougel, V.; Pucino, M.; Searles, K.; Yamamoto, K.; Zhizhko, P. A. Bridging the Gap between Industrial and Well-Defined Supported Catalysts. *Angew. Chem., Int. Ed.* **2018**, *57* (22), 6398−6440.

(39) Liu, L.; Corma, A. Isolated Metal Atoms and Clusters for Alkane Activation: Translating Knowledge from Enzymatic and Homogeneous to Heterogeneous Systems. *Chem* **2021**, *7* (9), 2347−2384.

(40) Zhang, Q.; Guan, J. Single-Atom Catalysts for Electrocatalytic Applications. *Adv. Funct. Mater.* **2020**, *30* (31), 2000768.

(41) Luo, E.; Zhang, H.; Wang, X.; Gao, L.; Gong, L.; Zhao, T.; Jin, Z.; Ge, J.; Jiang, Z.; Liu, C.; Xing, W. Single-Atom $Cr-N_4$ Sites Designed for Durable Oxygen Reduction Catalysis in Acid Media. *Angew. Chem., Int. Ed.* **2019**, *131* (36), 12599−12605.

(42) Chen, F.; Wu, X.; Shi, C.; Lin, H.; Chen, J.; Shi, Y.; Wang, S.; Duan, X. Molecular Engineering toward Pyrrolic N-Rich $M-N_4$ (M = Cr, Mn, Fe, Co, Cu) Single-Atom Sites for Enhanced Heterogeneous Fenton-Like Reaction. *Adv. Funct. Mater.* **2021**, *31* (13), 2007877.

(43) Gao, J.; Zheng, Y.; Tang, Y.; Jehng, J. M.; Grybos, R.; Handzlik, J.; Wachs, I. E.; Podkolzin, S. G. Spectroscopic and Computational Study of Cr Oxide Structures and Their Anchoring Sites on ZSM-5 Zeolites. *ACS Catal.* **2015**, *5* (5), 3078−3092.

(44) Dzwigaj, S.; Shishido, T. State of Chromium in CrSiBEA Zeolite Prepared by the Two-Step Postsynthesis Method: XRD, FTIR, UV−vis, EPR, TPR, and XAS Studies. *J. Phys. Chem. C* **2008**, *112* (15), 5803−5809.

(45) Tielens, F.; Islam, M. M.; Skara, G.; De Proft, F.; Shishido, T.; Dzwigaj, S. Chromium Sites in Zeolite Framework: Chromyl or Chromium Hydroxyl Groups? *Microporous Mesoporous Mater.* **2012**, *159*, 66−73.

(46) Li, Y.; Walsh, A. G.; Zhang, P.; Zhang, T. Heterogeneous Catalysis with Metal-Containing Crystalline Porous Materials: Element- and Site-Specific Insights. *CCS Chem.* **2024**, *6* (5), 1110−1129.

(47) van Bokhoven, J. A.; Lamberti, C. Structure of Aluminum, Iron, and Other Heteroatoms in Zeolites by X-Ray Absorption Spectroscopy. *Coordin Chem. Rev.* **2014**, *277−278*, 275−290.

(48) Zeng, L.; Cheng, K.; Sun, F.; Fan, Q.; Li, L.; Zhang, Q.; Wei, Y.; Zhou, W.; Kang, J.; Zhang, Q.; Chen, M.; Liu, Q.; Zhang, L.; Huang, J.; Cheng, J.; Jiang, Z.; Fu, G.; Wang, Y. Stable Anchoring of Single Rhodium Atoms by Indium in Zeolite Alkane Dehydrogenation Catalysts. *Science* **2024**, *383* (6686), 998−1004.

(49) Groppo, E.; Rojas-Buzo, S.; Bordiga, S. The Role of In Situ/Operando IR Spectroscopy in Unraveling Adsorbate-Induced Structural Changes in Heterogeneous Catalysis. *Chem. Rev.* **2023**, *123* (21), 12135−12169.

(50) Bordiga, S.; Lamberti, C.; Bonino, F.; Travert, A.; Thibault-Starzyk, F. Probing Zeolites by Vibrational Spectroscopies. *Chem. Soc. Rev.* **2015**, *44* (20), 7262−7341.

(51) Kunkeler, P. J.; Zuurdeeg, B. J.; van der Waal, J. C.; van Bokhoven, J. A.; Koningsberger, D. C.; van Bekkum, H. Zeolite Beta: The Relationship between Calcination Procedure, Aluminum Configuration, and Lewis Acidity. *J. Catal.* **1998**, *180* (2), 234−244.

(52) Dai, W.; Lei, Q.; Wu, G.; Guan, N.; Hunger, M.; Li, L. Spectroscopic Signature of Lewis Acidic Framework and Extraframework Sn Sites in Beta Zeolites. *ACS Catal.* **2020**, *10* (23), 14135−14146.

(53) Cavani, F.; Koutyrev, M.; Trifirò, F.; Bartolini, A.; Ghisletti, D.; Iezzi, R.; Santucci, A.; Del Piero, G. Chemical and Physical Characterization of Alumina-Supported Chromia-Based Catalysts

and Their Activity in Dehydrogenation of Isobutane. *J. Catal.* **1996**, *158* (1), 236−250.

(54) Ashuiev, A.; Giorgia Nobile, A.; Trummer, D.; Klose, D.; Guda, S.; Safonova, O. V.; Copéret, C.; Guda, A.; Jeschke, G. Active Sites in Cr(III)-Based Ethylene Polymerization Catalysts from Machine-Learning-Supported XAS and EPR Spectroscopy. *Angew. Chem., Int. Ed.* **2024**, *136* (1), No. e202313348.

(55) Trummer, D.; Searles, K.; Algasov, A.; Guda, S. A.; Soldatov, A. V.; Ramanantoanina, H.; Safonova, O. V.; Guda, A. A.; Copéret, C. Deciphering the Phillips Catalyst by Orbital Analysis and Supervised Machine Learning from Cr Pre-Edge XANES of Molecular Libraries. *J. Am. Chem. Soc.* **2021**, *143* (19), 7326−7341.

(56) Sun, P.; Liu, C.; Wang, H.; Liao, Y.; Li, X.; Liu, Q.; Sels, B. F.; Wang, C. Rational Positioning of Metal Ions to Stabilize Open Tin Sites in Beta Zeolite for Catalytic Conversion of Sugars. *Angew. Chem., Int. Ed.* **2023**, *62* (6), No. e202215737.

(57) Harris, J. W.; Cordon, M. J.; Di Iorio, J. R.; Vega-Vila, J. C.; Ribeiro, F. H.; Gounder, R. Titration and Quantification of Open and Closed Lewis Acid Sites in Sn-Beta Zeolites That Catalyze Glucose Isomerization. *J. Catal.* **2016**, *335*, 141−154.

(58) Qi, L.; Das, S.; Zhang, Y.; Nozik, D.; Gates, B. C.; Bell, A. T. Ethene Hydroformylation Catalyzed by Rhodium Dispersed with Zinc or Cobalt in Silanol Nests of Dealuminated Zeolite Beta. *J. Am. Chem. Soc.* **2023**, *145* (5), 2911−2929.

(59) Qi, L.; Babucci, M.; Zhang, Y.; Lund, A.; Liu, L.; Li, J.; Chen, Y.; Hoffman, A. S.; Bare, S. R.; Han, Y.; Gates, B. C.; Bell, A. T. Propane Dehydrogenation Catalyzed by Isolated Pt Atoms in ≡SiOZn−OH Nests in Dealuminated Zeolite Beta. *J. Am. Chem. Soc.* **2021**, *143* (50), 21364−21378.

(60) Buzzoni, R.; Bordiga, S.; Ricchiardi, G.; Lamberti, C.; Zecchina, A.; Bellussi, G. Interaction of Pyridine with Acidic (H-ZSM5, H-*β*, H-MORD Zeolites) and Superacidic (H-Nafion Membrane) Systems: An IR Investigation. *Langmuir* **1996**, *12* (4), 930−940.

(61) Emeis, C. A. Determination of Integrated Molar Extinction Coefficients for Infrared Absorption Bands of Pyridine Adsorbed on Solid Acid Catalysts. *J. Catal.* **1993**, *141* (2), 347−354.

(62) Lefton, N. G.; Bell, A. T. Effects of Structure on the Activity, Selectivity, and Stability of Pt-Sn-DeAlBEA for Propane Dehydrogenation. *ACS Catal.* **2024**, *14* (6), 3986−4000.